Lucjan Pająk*, Bożena Bierska-Piech*, J. Mrowiec-Białoń, A.B. Jarzębski, Ryszard Diduszko**

*** Institute of Materials Science, University of Silesia,** Bankowa 12, 40-007 Katowice, Poland

**** Industrial Institute of Electronics,** Długa 44/50, 00-241 Warszawa, Poland

SAXS from Particle and Disordered Systems

Abstract

SAXS studies were performed on different porous, disordered materials such as silica and zirconia aerogels, silica xerogels and carbonaceous materials (anthracite and shungite coals, coke, electrode material and activated carbon). These materials feature a variety of nanostructures. The relation between the profiles of the SAXS curves and the nanostructure of the materials was analysed. Fractal geometry proved to be very useful in this analysis. All types of fractality (mass, pore and surface fractality) were found in the materials studied. Porod plots appeared to be very sensitive to the structural details of the scattering objects.

Key words: *SAXS, particle size distribution, aerogels, xerogels, carbonaceous materials, fractals.*

Introduction

Methods based on scattering phenomena are very useful in studying materials which are heterogeneous in nanoscale [1-3], especially those exhibiting nanoporous structure. When the scattering regions are of the particle type, then calculations of size distributions can be performed from scattering when the following conditions are satisfied:

- both the scattering particles and the surrounding medium have uniform but different electron densities;
- the concentration of particles is low (generally below 5 vol.%);
- the scattering particles are of approximately the same, known shape;
- there is no order in the mutual location of particles, which means that the location of each particle does not depend on the positions of the others;
- there is no preferential orientation of particles of non-spherical shape with respect to primary beam direction.

Bierska *et al*. [4] analysed the influence of polydispersity and the size of the spherical particles on the calculated size distributions. The polydispersity P of the system of scattering spherical particles can be defined as a ratio of full width at half the maximum of the size distribution profile $D_v(R)$ (size distribution 'by volume') to the radius R_M of particles for which the size distribution has its main maximum. They found that the difference between the assumed (Gauss type) and calculated size distribution decreases with the increase of polydispersity and the size of the scattering particles. Moreover, the profile of assumed size distribution is maintained and the location of the main maximum of both size distributions is practically the same, irrespective of the polydispersity and size of the scattering particles.

The simulated SAXS intensities for the Gauss type profile of size distributions, calculated using the ITP software from Glatter [5], are presented in log $I(q)$ vs. log q plots (Figure 1a: R_M and P parameters are equal to 40 Å and 0.2, 0.5, 1.0 respectively), where the $I(q)$ is point-collimated scattering intensities, $q = 4\pi\sin\pi/\pi$, 2π - the scattering angle, and π is the X-ray wavelength. The Porod plots (Figure 1b) present the relation of $I(q)q^4$ vs. q. From Figure 1 it is clearly seen that for low polydispersity (P = 0.2), the Porod curve shows a distinct maximum which diminishes with the increase of the parameter P.

The interpretation of the scattering effect from complex, disordered materials notably simplifies when fractal geometry can be applied in the description of their structure. The SAXS intensity from fractal objects has a simple power-law form [1-3]:

$$I(q) = I_0 q^{-\alpha} \tag{1}$$

where I_o and a are constants.

The values of the power-law exponent α can be determined from the slope of linear parts of log $I(q)$ vs. log q plots. From these values, the mass (D_m), pore (D_p) and surface (D_s) fractal dimensions can be calculated.

For volume (mass or pore) fractals,

$$\alpha = D_m \text{ or } D_p, \text{ so } 1 < \alpha < 3 \quad \text{since } 1 < D_m \text{ or } D_p < 3, \tag{2}$$

whereas for surface fractals,

$$\alpha = 6\text{-}D_s \text{ so } 3 < \alpha < 4 \quad \text{since } 2 < D_s < 3. \tag{3}$$

The values of exponent a for both the volume and surface fractal do not overlap. This value may thus be used to dis-

Table 1. *Fractal characterization of the studied materials.*

Sample	Fractal dimension			Fractality range	
	D_m	D_p	D_s	a [Å]	ξ [Å]
Z1	2.25	-	-	24	> 280
	-	-	2.00	3.0	8.0
Z2	-	-	2.00	7.0	22
SA1	-	-	2.00	3.1	8.3
SX1	-	-	2.00	1.8	4.0
SX2	-	-	2.00	3.3	6.2
SX3	-	-	2.35	4.0	36
SX4	-	-	2.70	2.6	28
C1	-	1.50	-	1.8	25
C2	-	-	2.00	2.7	5.1
C3	-	2.75	-	3.4	89
C4	-	-	2.40	8.2	170
C5	-	-	-	-	-

tinguish whether the structure of scatterers is a volume or surface fractal. The above considerations are valid when scatterers show a narrow, 'bell' shape of polydispersity. The polydispersity of the power-law type affects the value of the exponent α considerably [2].

Generally, the deviations from the classical Porod law ($\alpha = 4.00$, $D_s = 2.00$) may be caused by:

- short-range electron density fluctuations within the solid phase,
- the roughness or fractal properties of pore-solid interface,
- a power-law pore size distribution (by number).

The self-similarity of real, physical objects can be satisfied only in a statistical sense, and most real objects can reveal fractal properties over a limited range of length:

$$\alpha < l < \xi. \qquad (4)$$

The ratio ξ/α can be regarded as the measure of fractality range. It is often postulated that 'good', physical fractals ought to show fractal properties over at least one order of magnitude for the ratio ξ/α. The values of α *and* ξ parameters correspond to the scale of the radius of gyration.

Materials and experiment

SAXS studies were performed on different porous materials:

Oxide porous materials: zirconia, silica and silica-titania gels were fabricated in the Materials Laboratory of Polish Academy of Sciences at Gliwice. Zirconia aerogels (Z1, Z2) were prepared as described in [6]. Z1 is the sample as obtained from high-temperature supercritical drying of wet gels, whereas Z2 is the same sample after 2 h calcination in air at 773 K.

The preparation of silica xerogel samples SX1, SX3 and SX4 was described most recently in [7]. SA1 is the aerogel prepared as SX1, but dried at supercritical conditions and not at ambient (as SX1). The synthesis protocol for highly porous silica-titania xerogels was devised earlier [8]. The SX2 sample contained 5 mol.% of TiO_2.

Carbonaceous materials: sample **C1** is a typical anthracite coal (Sverdlovsk [Ekaterinburg], Russia). **C2** sample is a carbon-rich shungite coal from Shunga in

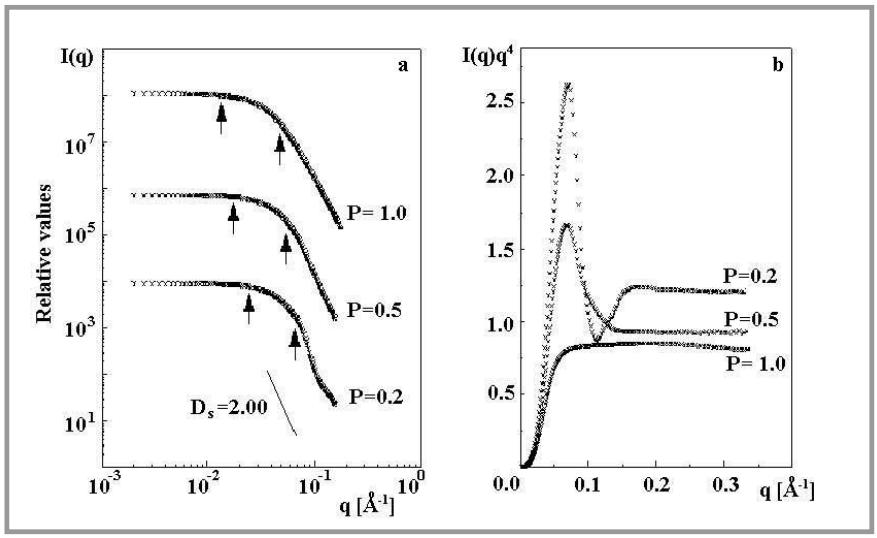

Figure 1. *Simulated SAXS intensities and Porod plots from a system of spherical particles for which R_M and P parameters equal 40 Å and 0.2, 0.5, 1.0 respectively.*

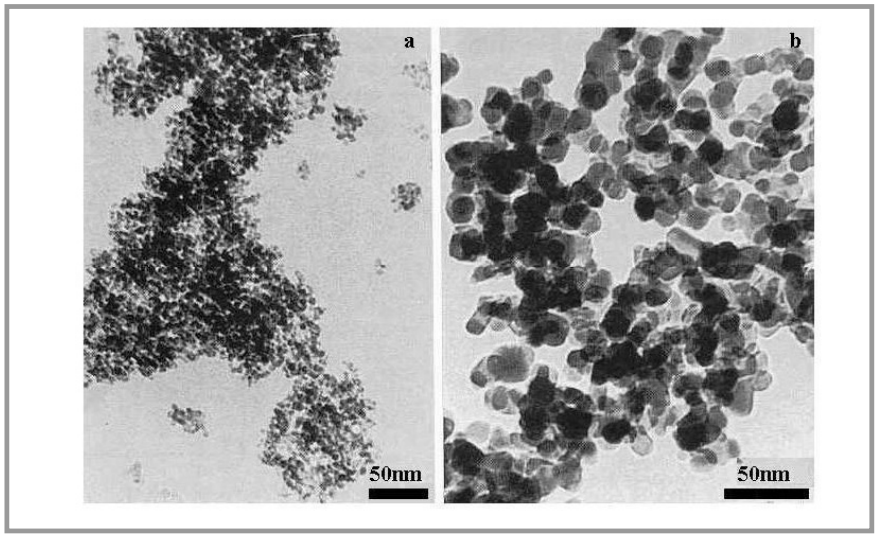

Figure 2. *TEM images of pre-prepared Z1 (a) and calcined Z2 (b) zirconia aerogel.*

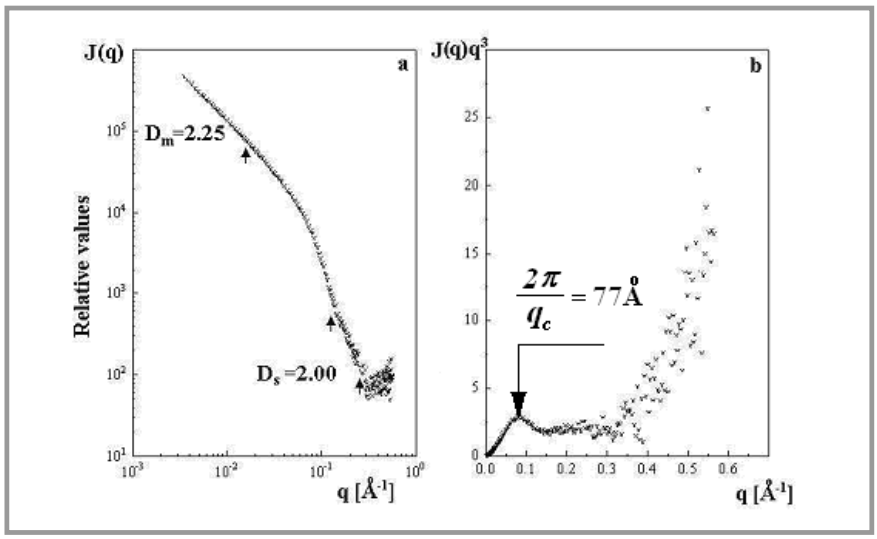

Figure 3. *Log I(q) vs. log q (a) and Porod (b) plots from pre-prepared zirconia aerogel (Z1).*

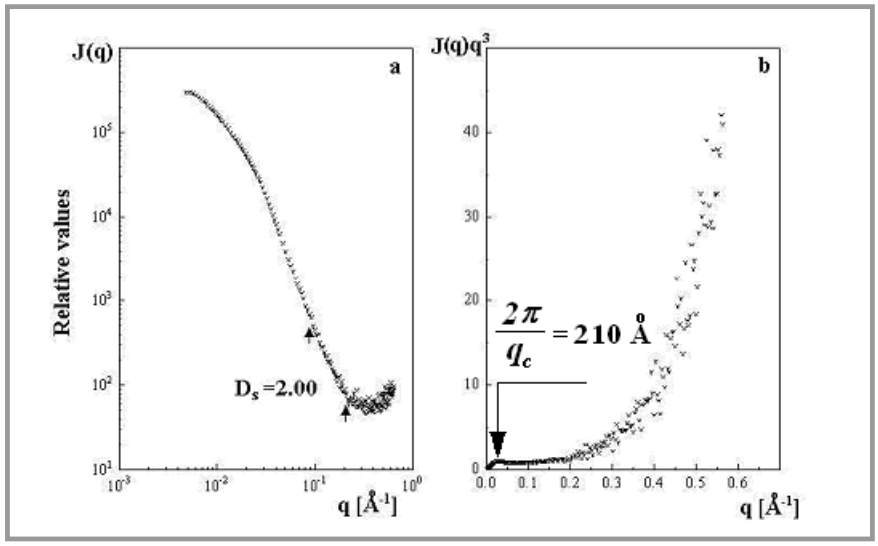

Figure 4. *Log I(q) vs. log q (a) and Porod (b) plots from calcined zirconia aerogel (Z2).*

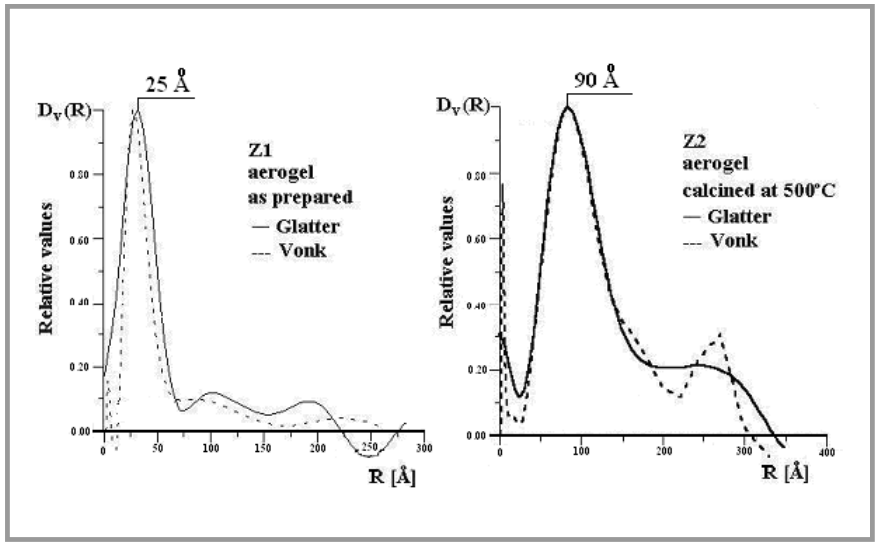

Figure 5. *Size distributions of primary particles in pre-prepared and calcined zirconia aerogel samples.*

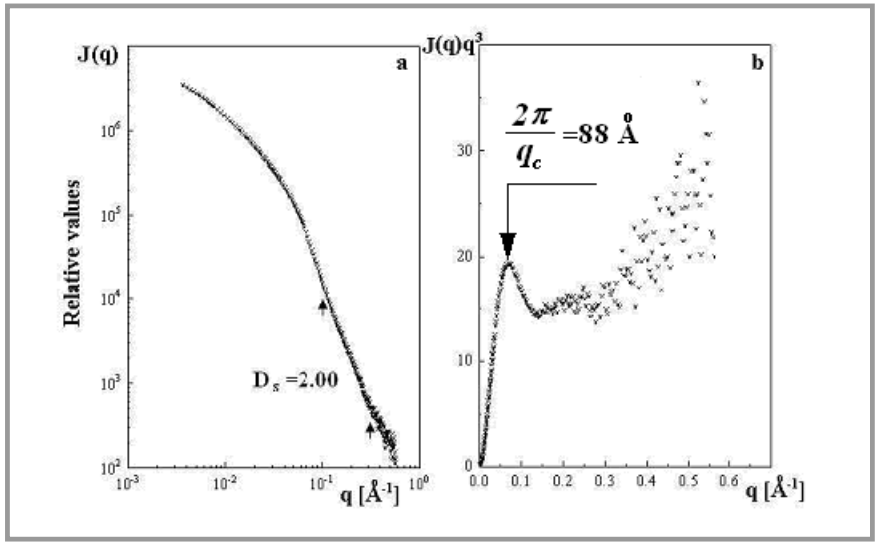

Figure 6. *Log I(q) vs. log q (a) and Porod (b) plots from silica aerogel (SA1 sample).*

the Karelia region of Russia. Some of these coals have carbon concentrations of up to 98 wt.%. It is interesting to note that a fullerene-like structure has been postulated for them as the globules found in these coals resemble those of giant fullerenes [9]. Sample **C3** is the coke taken from the tuyere level of blast furnace at the 'Katowice' Ironworks (Poland). Sample **C4** (synthetic graphite) applied as electrode material was produced by burning and graphitising the intermediate product from pitch and calcined coke, which play the roles of 'binder' and 'filler' respectively. The activated carbon prepared by carbonising saccharose is sample **C5**.

The SAXS experiments were carried out with a Kratky camera made by JEOL. Nickel-filtered Cu radiation, a scintillation counter and a pulse-height discriminator were used. The entrance and counter slits measured 100 and 300 mm respectively. Parasitic scattering on the collimation system was eliminated. In the present work, the scattering data are presented on log $J(q)$ vs. log q and Porod ($J(q)q^3$ vs. q) plots, where $J(q)$ is the SAXS intensity measured at 'infinitely-long' primary beam conditions. The slope of the linear part of the log-log plots strongly depends on the method of background correction, especially in the region of the large q parameter. The background was assumed constant throughout the whole q range, and was mainly caused by the short-range fluctuations in electron density; it was subtracted to obtain the best fit of the scattering data to the generalised power-law scattering. The values of exponent a of the power-law scattering, corresponding to the point collimation of the primary X-ray beam, were estimated from the relation $\alpha = \alpha^* + 1$. The values of α^* were determined from the slope of the linear part of log $J(q)$ vs. log q plots. All the samples studied were in the form of powder packed between two thin foils.

The influence of the preparation conditions of the investigated samples on their nanostructure is outside the scope of the present work.

Results and discussion

The results of the fractal analysis of the samples are presented in Table 1. From the location of the crossover points (marked in the figures by arrows), the limits of fractality range in real space (α, ξ) could be estimated [1-3] as follows:

$$a = \frac{1}{q_{max}} \quad (5)$$

$$\xi = \frac{1}{q_{min}} \quad (6)$$

The log $I(q)$ vs. log q curves show a linear section extending over at least one order of magnitude of the q parameter for Z1, SX3, SX4, C1, C3 and C4 samples. For the other samples, the fractality range is narrower.

Zirconia aerogels

Zirconia aerogels, both as prepared (Figure 2a) and after calcination (Figure 2b), are an aggregate of primary particles. The shape of these particles is very close to spherical. The SAXS curve of sample Z1 indicates the mass fractality of the primary particle aggregate with a mass fractal dimension $D_m = 2.25$ (Figure 3a). The mass fractality of the calcined sample Z2 is outside the range of q available in the applied SAXS experiment (Figure 4a). Primary particles of zirconia aerogels have a smooth and sharp pore-solid interface ($D_s = 2.00$). The increase in $J(q)q^3$ product at higher q values, which is more pronounced for the calcined sample, indicates the microporosity of primary particles. The size distributions (by 'volume' $D_v(R) - R$ is the radius of particles) calculated using the Glatter and Vonk methods [5, 10] are presented in Figure 5. Good agreement with the TEM images was obtained. It is interesting to note the local maximum of size distribution curves, which are more pronounced for the calcined sample, at low particle diameters ($R \approx 8$ Å). This maximum can be prescribed to micropores inside primary particles. On the other hand, the local maxima at higher R-values are probably the result of scattering from particle aggregates.

Silica gels

Figures 6-10 show a variety of SAXS curve profiles obtained from dry, silica gels. Differences between scattering curves are more clearly seen on the corresponding Porod plots. For SA1 silica aerogel (Figure 6), a distinct maximum on the Porod curve at low q indicates low polydispersity of primary particles (see Figure 1). According to Hasmy et al. [11], the averaged particle diameter can be determined ($a_o = 2\pi/q_c$) from the location q_c, of this maximum. The moderate increase in $J(q)q^3$ at higher q can be attributed to the poor microporosity of primary particles.

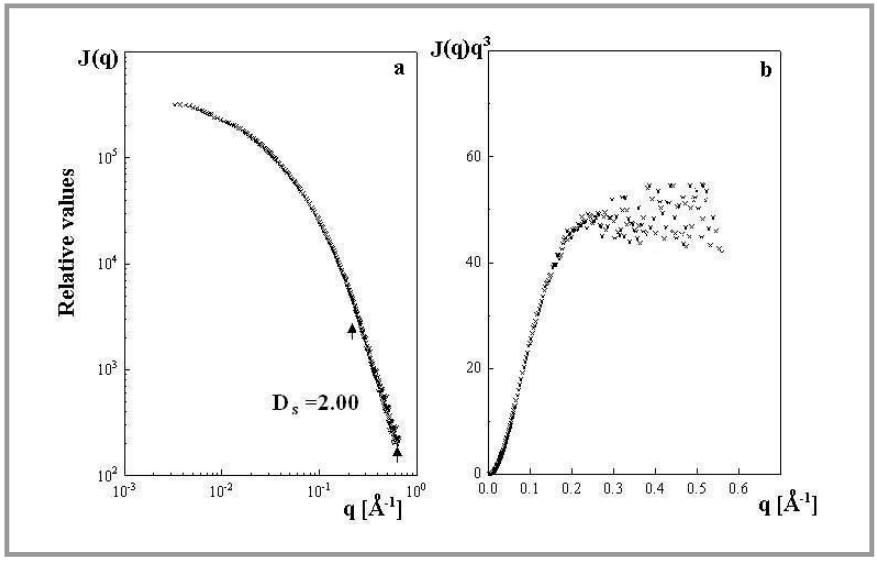

Figure 7. *Log I(q) vs. log q (a) and Porod (b) plots from silica xerogel (SX1 sample).*

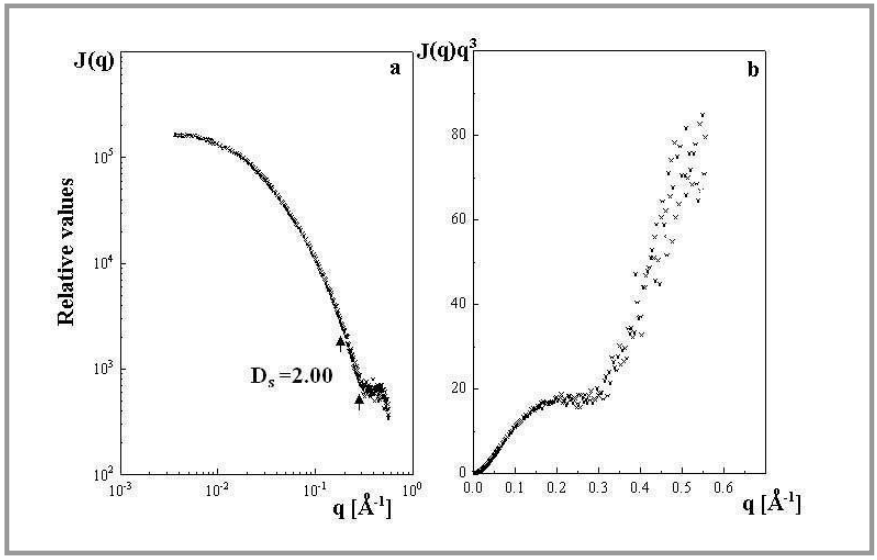

Figure 8. *Log I(q) vs. log q (a) and Porod (b) plots from silica xerogel (SX2 sample).*

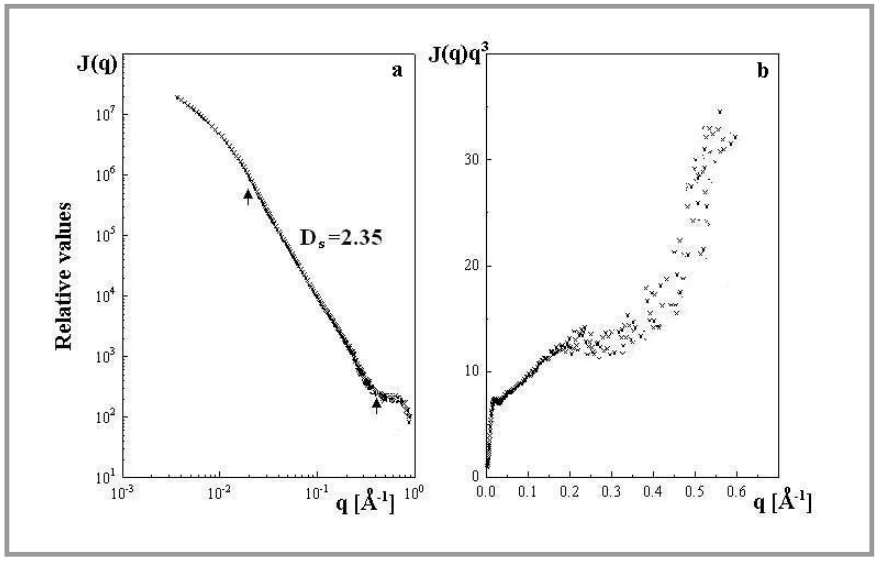

Figure 9. *Log I(q) vs. log q (a) and Porod (b) plots from silica xerogel (SX3 sample).*

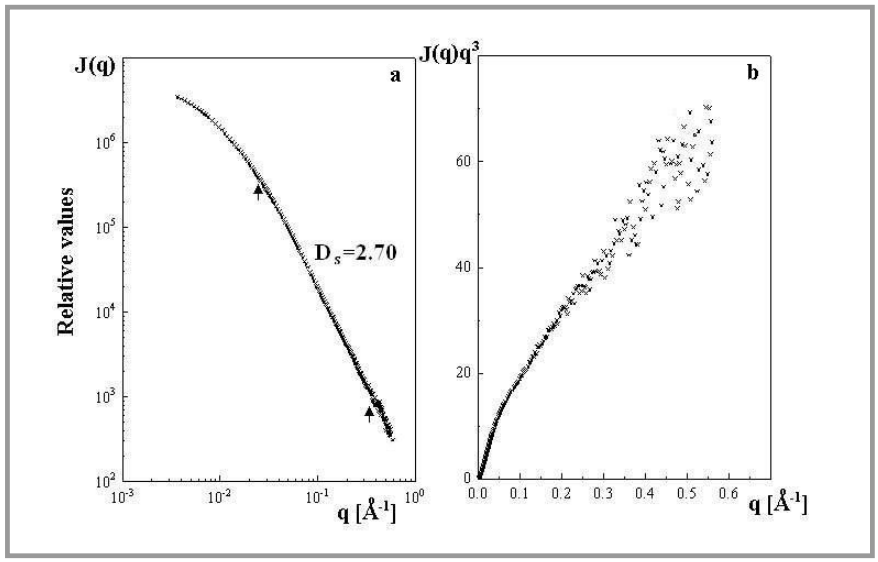

Figure 10. *Log I(q) vs. log q (a) and Porod (b) plots from silica xerogel (SX4 sample).*

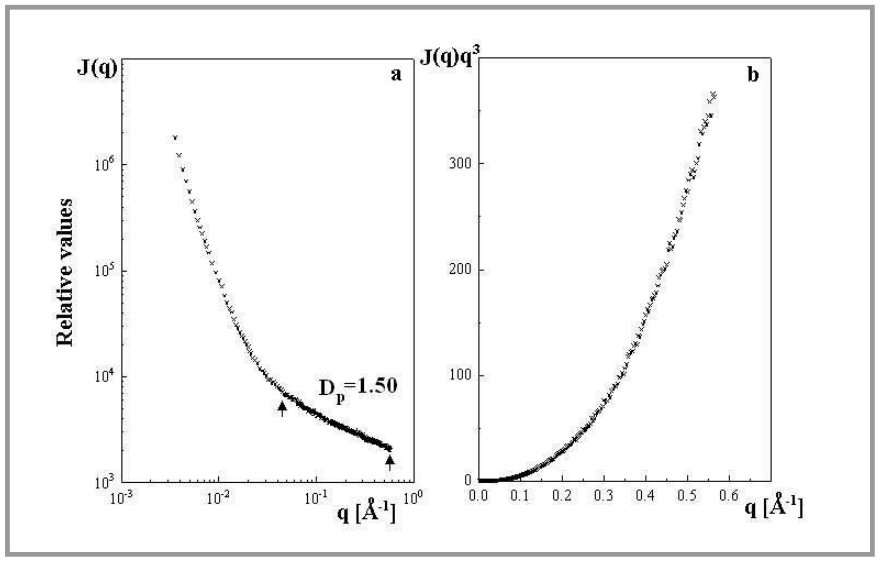

Figure 11. *Log I(q) vs. log q (a) and Porod (b) plots from anthracite (C1 sample).*

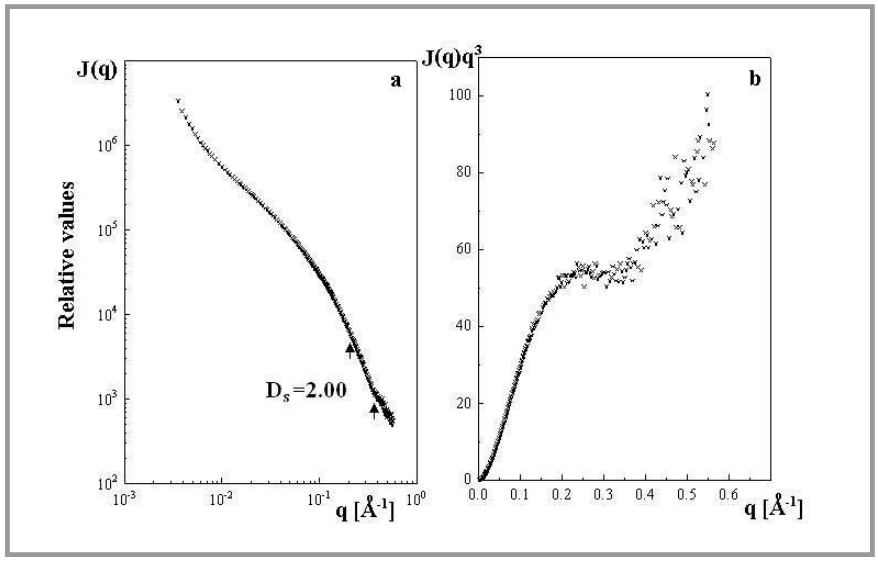

Figure 12. *Log I(q) vs. log q (a) and Porod (b) plots from shungite coal (C2 sample).*

The profile of the Porod curve from the SX1 silica xerogel (Figure 7) indicates the high polydispersity of primary particles without microporosity inside them. In turn, for the SX3 sample (Figure 8), both log $J(q)$ vs. log q and the Porod plots clearly indicate the scattering objects in two different scales of length. Primary particles of high polydispersity with distinct micropores inside them can be postulated in this sample.

The log $J(q)$ vs. log q plots for the two silica xerogels SX3 and SX4 (Figure 9 and 10) indicate the presence of surface fractality over a fairly large range of scales of length. This fractality range for sample SX4 extends up to the molecular length scale. The profiles of SAXS curves from SX3 xerogel (Figure 9) show the scattering regions in two different length scales: primary particles with a rough pore-solid interface, and micropores inside. The roughness of the pore-solid interface of sample SX3 (Figure 9a, $D_s = 2.35$) is lower than that of SX4 (Figure 10a, $D_s = 2.70$).

Carbonaceous materials

The most important aspect of carbonaceous materials is their microporous structure. Experimental data show significant differences in the structure of the carbonaceous materials studied (Figure 11–15). The Guinier range [12] is only observed for activated carbon (Figure 15a). The corresponding radius of gyration R_g is equal to 5.5 Å. Assuming the spherical shape of pores, this value of R_g corresponds to a pore diameter of 14.3 Å. In the region of higher angles, the scattering intensity does not obey the classical Porod law apart from in a narrow range for shungite coal (sample C2).

The first two carbonaceous materials are natural coals (anthracite C1 and shungite C2) with a similar level of metamorphism. However, their SAXS profiles are quite different. For anthracite C1, the SAXS curve indicates pore fractality at short length scales with a poor degree of ramification ($D_p = 1.50$) and relatively large scattering objects. In shungite coal C2 (Figure 12), an interglobular network of pores (without distinct fractality) and intraglobular microporosity are very likely. Some similarity between the Porod plots of shungite coal (Figure 12b) and those of silica xerogel SX2 (Figure 8b) is seen. It can thus be postulated that the nanostructures of both samples appears to be 'positive' – 'negative'.

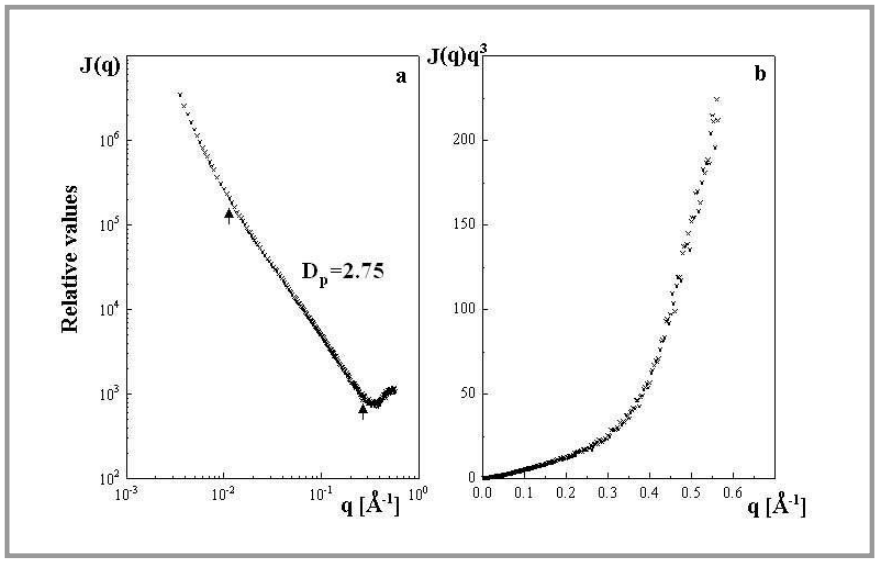

Figure 13. *Log I(q) vs. log q (a) and Porod (b) plots from coke (C3 sample).*

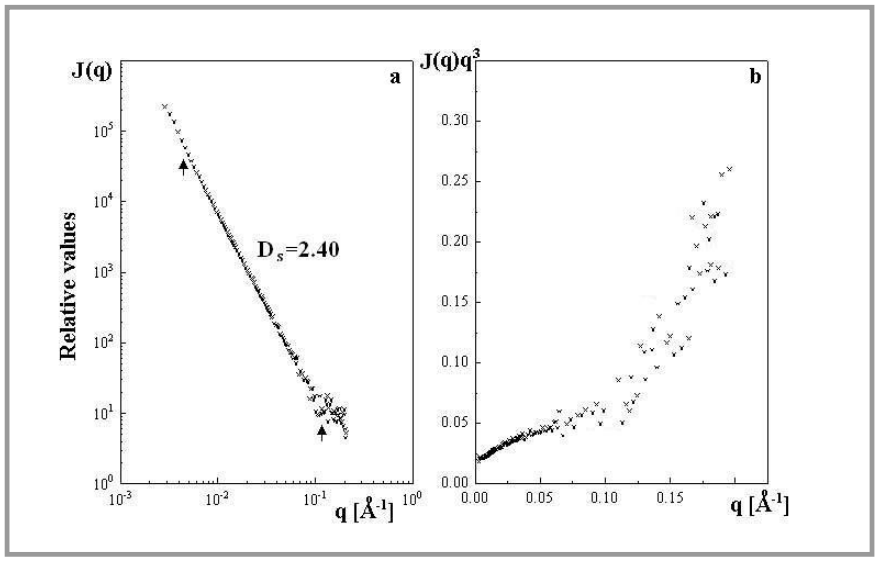

Figure 14. *Log I(q) vs. log q (a) and Porod (b) plots from electrode material (C4 sample).*

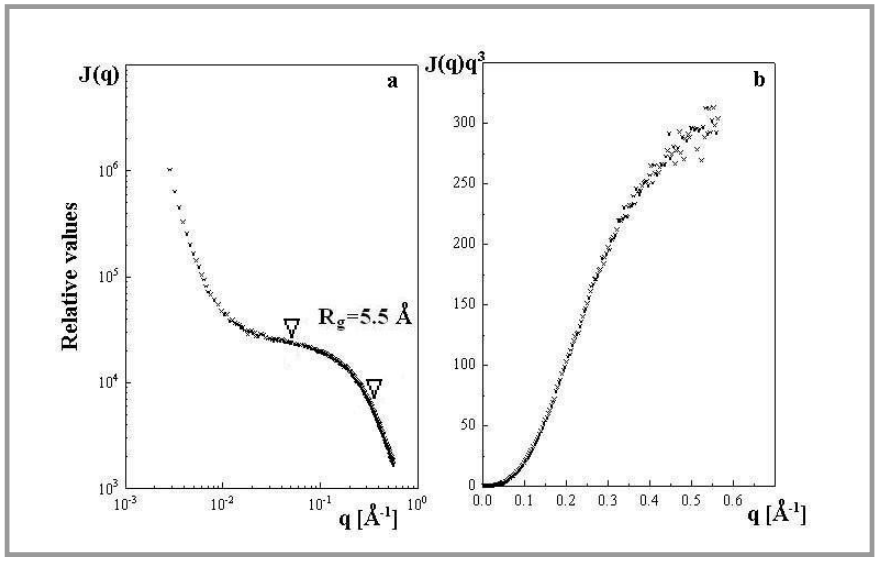

Figure 15. *Log I(q) vs. log q (a) and Porod (b) plots from activated carbon (C5 sample).*

For coke C3 (Figure13), the structure of pores can be described by pore fractality with relatively high pore fractal dimension (D_p = 2.75). On the other hand, for electrode material C4 (Figure 14), surface fractality and microporosity of the solid phase is observed. The SAXS curve profile for activated carbon C5 (Figure 15) indicates the presence of microporosity of the solid phase and larger scattering objects.

Conclusions

From the results obtained, a number of general conclusions can be drawn:

- Depending on the origin and the preparation conditions, the nanostructure of porous materials varies considerably.
- Owing to great distribution in size and shape of the scattering objects, the Guinier approximation is very rarely obeyed in porous materials.
- The classical Porod law indicating smooth and sharp pore-solid interfaces was satisfied in a narrow *q* range in all the porous materials studied.
- Fractal geometry appeared to be useful in the description of the morphology of the porous materials studied.

❑

References

1. *J.E. Martin, A.J. Hurd; J.Appl.Cryst.,* ***20****, 61 (1987)*
2. *P.W. Schmidt; J. Appl. Cryst.,* ***24****, 414 (1991)*
3. *J. Teixeira; J. Appl. Cryst.,* ***21****, 781 (1988)*
4. *B. Bierska, R. Diduszko, L. Pająk; Proc. of the XIXth Conference on Applied Crystallography, ed. H. Morawiec & D. Stróż, World Scientific, Singapore, pp. 51-54 (2004)*
5. *O. Glatter; J. Appl. Cryst.,* ***13****, 7 (1980)*
6. *J. Mrowiec-Białoń, L. Pająk, A.B. Jarzębski, A.I. Lachowski, J.J. Malinowski; J. Non-Cryst. Sol.,* ***225****, 115 (1998)*
7. *J. Mrowiec-Białoń, A.B. Jarzębski, L. Pająk, Z. Olejniczak, M. Gibas; Langmuir,* ***20****, 10389 (2004)*
8. *J. Mrowiec-Białoń, A.B. Jarzębski, O.A. Kholdeeva, N.N. Trukhan, V.I. Zaikovski, V.V. Kriventsov, Z. Olejniczak; Appl. Catal. A,* ***273****, 47 (2004)*
9. *V.V. Kovalevski, N.N. Rozkhova, A.Z. Zidenberg, A.N. Yermolin; Mol. Mat.* ***4****, 77 (1994)*
10. *C.G. Vonk; J. Appl. Cryst.,* ***9****, 433 (1976)*
11. *A. Hasmy, R. Vacher, R. Julien; Phys. Rev. B,* ***50****, 1305 (1994)*
12. *A. Guinier, G. Fournet; Small-Angle Scattering of X-Rays, John Wiley and Sons, New York, 1955*

❑ ***Received 08.12.2004 Reviewed 10.02.2005***